



# Integrative analysis of co-expression pattern of solute carrier transporters reveals molecular subtypes associated with tumor microenvironment hallmarks and clinical outcomes in colon cancer

Rui Zhou <sup>a,b,1</sup>, Lingbo Li <sup>a,1</sup>, Yue Zhang <sup>a,1</sup>, Zhihong Liu <sup>a,b</sup>, Jianhua Wu <sup>a,b</sup>, Dongqiang Zeng <sup>a,b</sup>, Huiying Sun <sup>a,b</sup>, Wangjun Liao <sup>a,b,\*</sup>

<sup>a</sup> Department of Oncology, Nanfang Hospital, Southern Medical University, Guangzhou, Guangdong, PR China

<sup>b</sup> Guangdong Province Key Laboratory of Molecular Tumor Pathology, Guangzhou, Guangdong, PR China

## ARTICLE INFO

### Keywords:

Solute carrier transporters  
Molecular subtype  
Colon cancer  
Prognosis  
Therapeutic outcome

## ABSTRACT

Recent findings have suggested that solute carrier (SLC) transporters play an important role in tumor development and progression, and alterations in the expression of individual SLC genes are critical for fulfilling the heightened metabolic requirements of cancerous cells. However, the global influence of the co-expression pattern of SLC transporters on the clinical stratification and characteristics of the tumor microenvironment (TME) remains unexplored. In this study, we identified five SLC gene subtypes based on transcriptome co-expression patterns of 187 SLC transporters by consensus clustering analysis. These subtypes, which were characterized by distinct TME and biological characteristics, were successfully employed for prognostic and chemotherapy response prediction in colon cancer patients, as well as demonstrated associations with immunotherapy benefits. Then, we generated an SLC score model comprising 113 genes to quantify SLC gene co-expression patterns and validated it as an independent prognostic factor and drug response predictor in several independent colon cancer cohorts. Patients with a high SLC score possessed distinct characteristics of copy number variation, genomic mutations, DNA methylation, and indicated an SLC-S2 subtype, which was characterized by strong stromal cell infiltration, stromal pathway activation, poor prognosis, and low predicted fluorouracil and immunotherapeutic responses. Furthermore, the analysis of the Cancer Therapeutics Response Portal database revealed that inhibitors targeting PI3K catalytic subunits could serve as promising chemosensitizing agents for individuals exhibiting high SLC scores. In conclusion, the co-expression patterns of SLC transporters aided the disease classification, and the SLC score proved to be a reliable tool for distinguishing SLC gene subtypes and guiding precise treatment in patients with colon cancer.

\* Corresponding author. Department of Oncology, Nanfang Hospital, Southern Medical University, 1838 North Guangzhou Avenue, Guangzhou, 510515, PR China.

E-mail address: [nfyyliaowj@163.com](mailto:nfyyliaowj@163.com) (W. Liao).

<sup>1</sup> These authors are contributed equally.

<https://doi.org/10.1016/j.heliyon.2023.e22775>

Received 14 December 2022; Received in revised form 9 November 2023; Accepted 19 November 2023

Available online 30 November 2023

2405-8440/© 2023 Published by Elsevier Ltd. This is an open access article under the CC BY-NC-ND license (<http://creativecommons.org/licenses/by-nc-nd/4.0/>).

## 1. Introduction

Solute carrier (SLC) transporters are the second largest superfamily of membrane proteins, comprising of 456 members that are grouped into 52 subfamilies according to their genetic sequence resemblance [1,2]. Physiologically, as gatekeepers of the cellular context, SLC family proteins mainly function to mediate the transport of substances along a concentration gradient, establishing their pivotal role in maintaining cellular homeostasis [2]. In tumor cells, SLC transporters are involved in modulation of diverse malignant behaviors, such as tumor invasion, metastasis, and drug resistance, which can be dependent on or independent of their primary function in influx/efflux [3–5]. Their dramatic expression alteration induced by the dysregulation of oncogenes and tumor suppressors is considered the premise of their tumor promoting or suppressing function [4]. Along with their effect on tumor cells, SLC transporters are considered a bridge between tumor cells and the tumor microenvironment (TME) [6]. Individual SLC transporters expressed on diverse immune cell types have been discovered to be able to control the differentiation, function, and destiny of these cells through modulation of a wide range of metabolic pathways [7]. Thus, SLC transporters may be considered as novel targets for modulating the immune response in the TME. However, although different SLC transporters have been reported to accomplish many complex biological functions by comprising a coordinated network [4], most studies have focused their attention on only one or two SLC transporters because of technical limitations. Therefore, it is imperative to explore molecular subtypes of tumours based on the expression profiles of SLC transporters from a broader perspective.

Colon cancer is the second leading cause of cancer-related mortality worldwide [8]. Although previous efforts have attempted to identify several predictive molecular biomarkers [9], the clinical stratification of patients with non-metastatic colon cancer who undergo radical resection is still solely based on the pathological TNM stage, in which T represents the size of the tumor, N represents the involved lymph nodes, and M represents distant metastasis. Recent studies have suggested that ctDNA is advantageous for predicting the prognosis and guiding the performance of adjuvant chemotherapy [10–12]. However, because of the high detection cost of ctDNA, its introduction into daily practice is difficult. Therefore, further investigation is required to identify classifiers that are more efficacious and accessible for clinical use.

To address these gaps in the research, we comprehensively evaluated the expression patterns of SLC family genes and identified a novel SLC gene expression-based molecular subtyping system. Moreover, a scoring scheme comprising 113 genes was established to quantify SLC gene co-expression patterns.

## 2. Materials and methods

### 2.1. Bulk transcriptomic data collection and processing

Previously described methods were used to obtain publicly accessible bulk transcriptomic data and pertinent clinical details of non-metastatic colon cancer patients were retrieved from the Gene Expression Omnibus (GEO, <https://www.ncbi.nlm.nih.gov/geo/>, GSE17538, GSE33113, GSE37892, GSE38832, and GSE39582) and The Cancer Genome Atlas (TCGA, <https://cancergenome.nih.gov/>, TCGA-COAD) databases [13,14]. The *affy* and *simpleaffy* packages were used to renormalize microarray data generated from the GPL570 platform, and the *sva* R package was used to merge different transcriptomic datasets. Regarding the processing of RNA sequencing data, the *voom* algorithm was used to convert count data into values similar to those from microarrays. Additionally, we obtained *voom*-transformed RNA sequencing data from the databases of Sun Yat-sen University Cancer Center (SYSUCC), comprising 30 patients who were diagnosed with non-metastatic colon cancer, as detailed in prior research [13,14].

### 2.2. Single-cell RNA sequencing (scRNA-seq) data collection and processing

The public scRNA-seq dataset GSE188711 was downloaded [15] and processed using the Seurat R package. We first removed unqualified cells/genes that fit the following criteria: gene count per cell <300, genes expressed in fewer than three cells, percentage of mitochondrial genes per cell >20, and percentage of ribosomal genes per cell >3. After normalizing the data by using the Log-Normalize method, we subsequently utilized the *FindVariableFeatures* function incorporated in the Seurat package to obtain the top 3000 most highly variable genes among the cells, which were used in the subsequent principal component analysis (PCA) to reduce data dimensions. Then, the PCA method was utilized to reduce the data dimension by setting the number of principal components as 10 and the *FindNeighbors* and *FindClusters* functions were employed to obtain the nearest neighbors and major cell clusters, respectively. Cell clusters were visualized using the uniform manifold approximation and projection (UMAP) algorithm. All cluster assignments underwent manual verification to ensure the precise partitioning of cells. The *InferCNV* and *CopyKAT* packages were used to identify malignant epithelial cells. The malignant and non-malignant epithelial cells were defined by intersecting the prediction results obtained by the *inferCNV* algorithm and the *CopyKat* algorithm. In particular, the prediction of malignant epithelial cells by *inferCNV* algorithm was achieved by simultaneously calculating “CNV score” and “CNV correlation” according to the method proposed by Lei Zhang et al. [16].

### 2.3. Identification of SLC gene subtypes by consensus clustering

We employed unsupervised clustering analysis (K-means) to characterize the expression pattern of SLC family genes based on their transcriptional profiling. To determine the most appropriate cluster number and estimate the clustering stability among all categories, the R package *ConsensusClusterPlus* was employed with the following settings: *maxK* = 10, *reps* = 1000, *pItem* = 0.95, and *pFeature*

= 1.

#### 2.4. Generation of the SLC score

The SLC score was established in two steps. First, the limma package was utilized for analyzing the differentially expressed genes (DEGs) between SLC-S2 and non-SLC-S2 subtypes in the GSE39582 cohort. The criterion used to determine DEGs was defined as the absolute "Log2FC" value greater than 1 and the adjusted P-value less than 0.01. We then used the Boruta algorithm incorporated in the Boruta package to reduce the dimensions of the DEGs that exhibited upregulation (gene cluster A) or downregulation (gene cluster B) in the SLC-S2 subtype. The Boruta algorithm was configured with the following parameters: doTrace = 2, maxRuns = 100, and ntree = 500, as previously described [14]. The final formula of the SLC score was: SLC score = (the average expression of the final determined gene cluster A) – (the average expression of the final determined gene cluster B).

#### 2.5. TME deconvolution and biological process analysis

Tumor microenvironment deconvolution was achieved using the single-sample gene set enrichment analysis (ssGSEA) algorithm incorporated in the GSVA R package. A total of twenty-three gene sets including stromal cells, myeloid cells, and lymphocytes were collected from relevant literature [17,18]. The infiltration level of various cell types was determined by utilizing gene transcriptional profiles to calculate the enrichment score of the gene set in a sample output obtained from the ssGSEA analysis. Biological process analysis was performed by employing GSVA on a compilation of fifty hallmark biological pathways collected from the Molecular Signature Database (<http://www.gsea-msigdb.org>).

#### 2.6. Multi-omics analysis

The multi-omics analysis conducted in this study contained copy number variation (CNV) analysis, somatic genetic mutation analysis, DNA methylation analysis, and proteomics analysis. For CNV analysis, the TCGAbiolinks package was employed to acquire the masked copy number segment data of patients. We performed GISTIC 2.0 analysis of the acquired CNV fragments by using GenePattern with the default settings. The TCGAbiolinks package was utilized to download the genetic mutation file, followed by the identification of significant cancer mutated genes (SMGs) using the MutSigCV algorithm ( $q < 0.05$ ) [19]. Subsequently, we focused on the top 100 SMGs based on their total mutation frequency and conducted a chi-square test to examine the distribution of effective mutations among these SMGs across different groups. For DNA methylation analysis, we obtained level three DNA methylation (Methylation450k) data from the UCSC Xena database and performed data preprocessing employing the ChAMP package. DNA methylation values were assigned to each gene by calculating the median beta value of the probes located in the promoter region. Subsequently, by employing the Kruskal-Wallis test, the top 1000 genes exhibiting the highest variance in methylation value ( $\beta$  values) were chosen as potential candidates for investigating different methylation genes between distinct groups. In addition, we also examined the transcriptomic expression variability of the aforementioned candidate genes across different groups and explored the correlation between the transcriptomic expression level and methylation level of each gene. The Benjamini-Hochberg correction was utilized for the multiple testing of adjusted  $-value$ . Finally, we designated significantly varied methylation genes (SVMGs) according to the following standards: both the methylation value and the corresponding transcriptional expression value of SVMGs exhibited significant variation between different groups (adjusted  $p$ -value  $< 0.05$ ), and a significant negative correlation could be observed between the methylation value and the corresponding transcriptional expression value of each SVMG (adjusted  $p$ -value  $< 0.05$ ).

#### 2.7. Therapeutic response prediction

Drug sensitivity was predicted by utilizing the Cancer Therapeutics Response Portal (CTRP) database [20] using the pRRophetic package. The quantification of drug sensitivity was accomplished by assessing the area under the dose-response curve (AUC), whereby lower AUC values were indicative of heightened sensitivity. In addition, we employed tumor immune dysfunction and exclusion (TIDE, <http://tide.dfci.harvard.edu>) [21] and SubMap algorithms to predict the immune checkpoint blockade (ICB) response of patients. The SubMap algorithm was implemented using the online module of the GenePattern website (<https://cloud.genepattern.org/>), and the transcriptomic data of the IMvigor210 cohort, which contains data regarding metastatic urothelial cancer patients receiving anti-PD-L1 therapy, was utilized for similarity comparison of transcriptional profiles.

#### 2.8. Statistical analysis

The Student's  $t$ -test was employed to assess disparities in normally distributed continuous variables between the two groups. When comparing differences between continuous variables that are not normally distributed, the Mann-Whitney  $U$  test was utilized instead. Chi-square and Fisher's exact tests were used to estimate the statistical significance of the differences between categorical variables. The correlations between continuous variables that were normally distributed and those that were not normally distributed were examined using Pearson and Spearman correlation tests, respectively. Survival curves were determined using the Kaplan-Meier algorithm and compared using the log-rank test. Hazard ratios for clinical variables were calculated through the execution of univariate and multivariate Cox regression analyses. All statistical analyses were conducted utilizing R software version 4.0.2 or SPSS version 25.0 (IBM Corp., Armonk, N.Y., USA). Two-sided statistical tests were conducted to test for significance, and the level of significance

was set at P value less than 0.05.

### 3. Results

#### 3.1. Overview of SLC family genes in colon cancer

The workflow of this study is shown in Fig. S1. The first step was to filter the gene members of the SLC family included for molecular subtyping. Thus, we started by integrating the expression matrix of 356 SLC family genes collected from *meta*-GEO and TCGA-COAD cohorts, among which 114 SLC family genes with an average expression of less than 4.0 were eliminated. Moreover, to elucidate the distribution of SLCs in tumor cells and immune cells in the TME, we obtained the single-cell sequencing data of GSE188711, which resolved the difference between left- and right-sided colon cancer via single-cell sequencing. Based on UMAP clustering analysis, all cells were categorized into eight major cell types, including fibroblasts, monocytes and macrophages, T cells, B cells, plasma cells, endothelial cells, undefined immune cells, and epithelial cells (Fig. 1A). The gene markers for each cell type are shown in Fig. 1B. We then obtained the expression matrix of the above 242 SLC molecules of each cell type and eliminated 55 SLC molecules whose mean expression abundance was less than 0.05 in all cell types. Finally, a total of 187 SLC transporters remained and Table S1 summarizes the cell functions and main subcellular locations of these SLC family members. We further explored the correlation between the

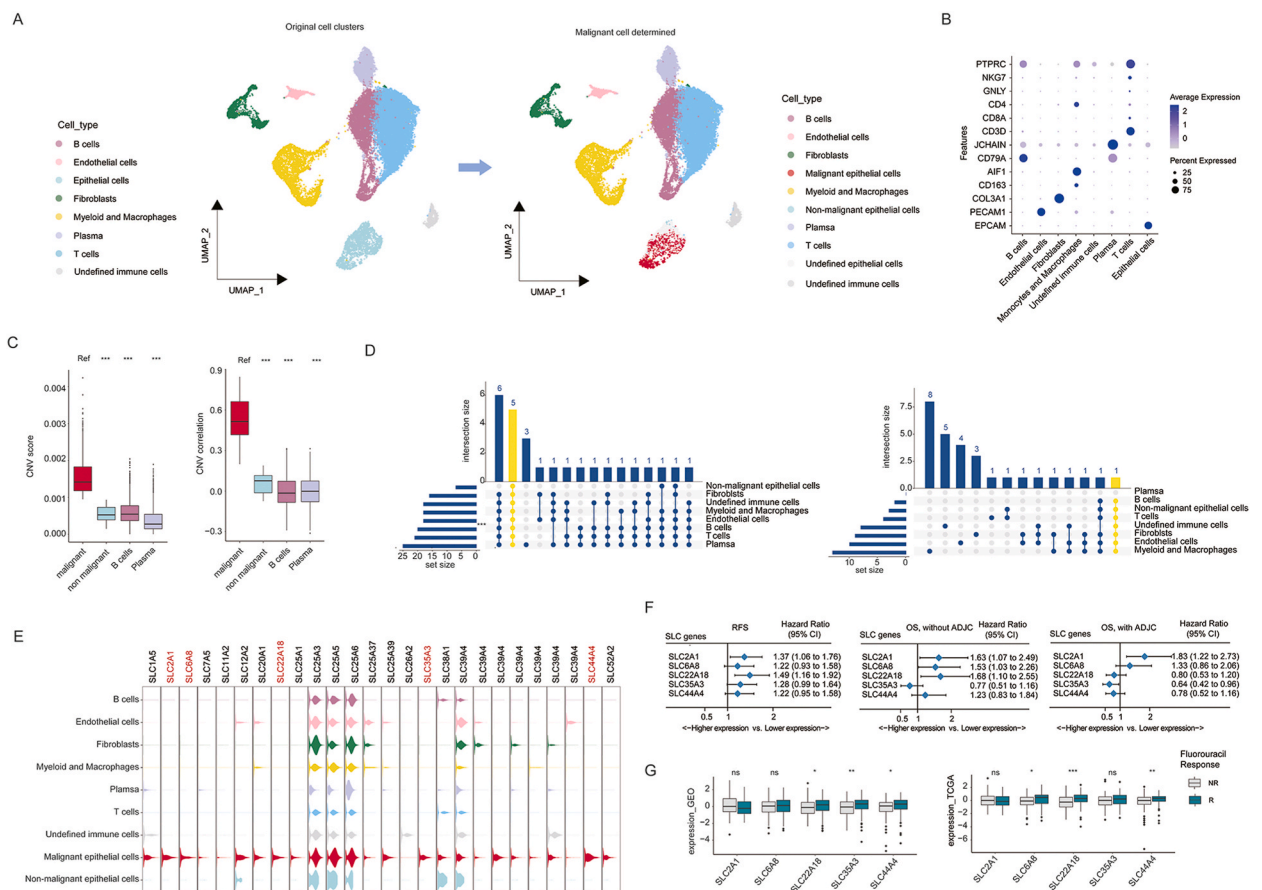


**Fig. 1.** The overview of the SLC family genes in colon cancer (A) UMAP plot of cells from colon cancer patients revealing eight clusters. Each cluster was shown in different colors. (B) Dot plots showing the average expression of known markers in indicated cell clusters. The expression intensity of markers is shown. (C) Boxplot showing the CNV score and CNV correlation in different cell clusters. Boxes represent 25–75 % of values, lines in boxes represent median values, whiskers represent 1.5 interquartile ranges, and black dots represent outliers. (D) Upset plot displaying the intersection of the upregulated (left) or downregulated (right) SLC genes in the tumor cells in comparison to other cell clusters. (E) Violin plots showing the expression of SLC family genes in tumor cells and immune cell clusters. (F) Forest plot displaying the unadjusted hazard ratios and 95 % confidence intervals of the five tumor cell-enriched SLC genes for relapse-free survival and overall survival in the *meta*-GEO cohort. (G) Boxplot showing the expression of five tumor cell-enriched SLC genes in fluorouracil responsive and non-responsive groups in the *meta*-GEO cohort and in the TCGA-COAD cohort. Boxes represent 25–75 % of values, lines in boxes represent median values, whiskers represent 1.5 interquartile ranges, and black dots represent outliers. *SLC*, solute carrier; *CI*, confidence interval; *ADJC*, adjuvant chemotherapy; *RFS*, recurrence-free survival; *OS*, overall survival; *R*, response; *NR*, nonresponse; and *CNV*, copy number variations. (For interpretation of the references to color in this figure legend, the reader is referred to the Web version of this article.)

expression levels of these 187 SLC transporters in colon cancer tissues. Consistent with previous studies, SLC transporters also exhibited specific co-expression patterns (Fig. S2), suggesting that these molecules may also have a synergistic biological role in the progression of colon cancer.

To explore the distribution of the above 187 SLC transporters in different cell types, we respectively defined cells with malignant and non-malignant phenotypes in the epithelial cell clusters (Fig. 1A) based on the inferCNV (Fig. 1C) and CopyKat algorithms (Fig. S3A). By comparing the expression differences of SLC family genes between malignant epithelial cells and other cell clusters, we identified several upregulated SLC genes in malignant cells (adj p value < 0.01). Among them, a total of five SLC genes, including *SLC2A1*, *SLC6A8*, *SLC22A18*, *SLC35A3*, and *SLC44A4*, were significantly upregulated in malignant epithelial cells and their expression was almost absent in all other non-malignant cell-types (Fig. 1D and E). Thus, we defined these genes as tumor cell-enriched SLC transporters. However, in terms of SLC genes that were enriched in non-tumor cells, only *SLC2A3* was highly expressed in all non-tumor cell populations except plasma cells, and it was expressed only slightly in tumor cells (Fig. S3). We then used bulk transcriptome data obtained from samples of the meta-GEO and TCGA-COAD cohorts to explore the potential correlation of expression levels of the above five tumor cell-enriched SLC transporters with patient prognosis and chemotherapy sensitivity. Results demonstrated that the elevated expression of the above five SLC genes predicted a higher risk of recurrence, while *SLC2A1* and *SLC22A18* showed statistical significance (Fig. 1F). However, as for overall survival, only the expression level of *SLC2A1* was significantly correlated with survival time in both the adjuvant chemotherapy performed and unperformed subgroups (Fig. 1F). Finally, regarding chemotherapeutic sensitivity analysis (Fig. 1G), we discovered that, compared with the fluorouracil non-responsive group, the expression of the above tumor cell-specific SLC transporters, except for *SLC2A1*, tended to be downregulated in samples of the fluorouracil non-responsive group, among which *SLC22A18* and *SLC44A4* showed significant differences in the meta-GEO and TCGA-COAD cohorts. Information about these five tumor cell-enriched SLC transporters and their involvement in colon cancer based on a literature review is provided in Table S2.

### 3.2. Identification of molecular subtypes mediated by the co-expression pattern of

#### 3.2.1. SLC family genes

As SLC transporters were co-expressed in colon cancer tissue, and the expression of individual transporters was correlated with patient clinical outcomes, we speculated whether patients could be classified by the expression of these 187 SLC transporters. Thus, unsupervised clustering analysis based on the transcriptional profiling of 187 SLC transporters in the meta-GEO cohort was performed (Tables S3–4). As shown in Fig. 2A, five clusters achieved the best clustering efficacy, which were denoted as SLC-S1 to SLC-S5 in

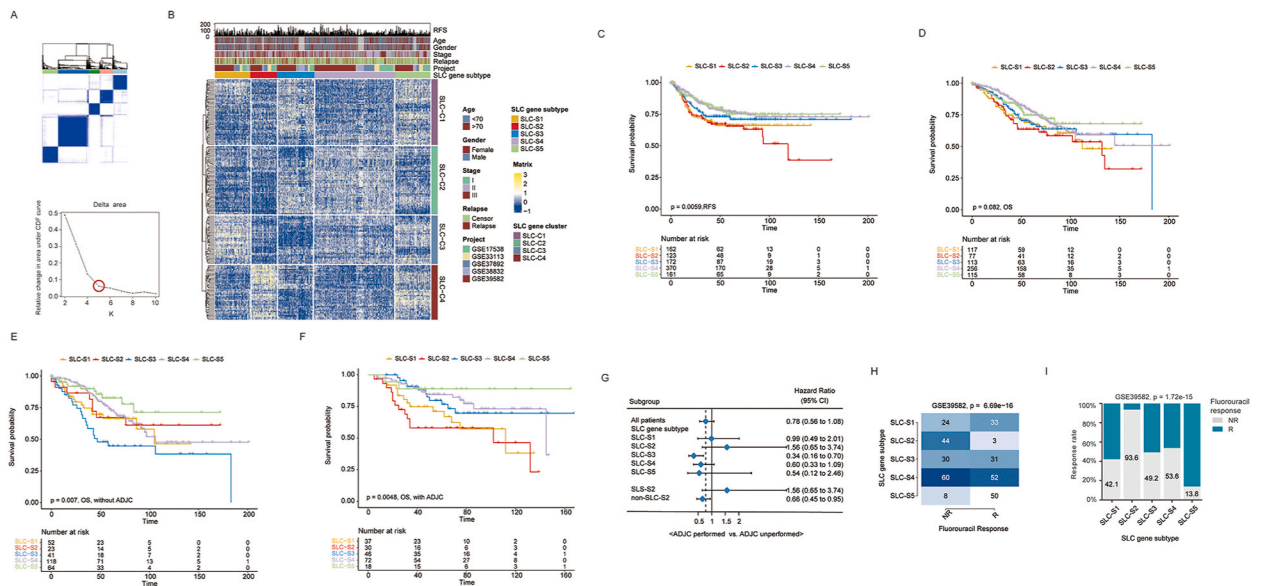


**Fig. 2.** Consensus clustering based on the expression of SLC family genes in colon cancer. (A) Consensus matrix (upper) and line chart (down) revealed that five clusters achieve the best clustering efficacy. (B) Heatmap shows the SLC gene subtypes in patients with colon cancer identified by the unsupervised clustering analysis of 187 SLCs in the integrated meta-GEO cohort. Cohort details are used as annotations. (C–D) Kaplan–Meier curves of relapse-free survival (C) and overall survival (D) according to SLC gene subtypes in the meta-GEO cohort. (E–F) Kaplan–Meier curves of overall survival according to SLC gene subtypes in the patient subgroup without (E) or with adjuvant chemotherapy (F) in the GSE39582 cohort. (G) Forest plots of benefits of adjuvant chemotherapy in different SLC gene subtypes in the GSE39582 cohorts. (H) Heatmap showing the fluorouracil response rates among five SLC gene subtypes. (I) Bar charts summarize the proportions of patients with fluorouracil-response signatures and those with nonresponse signatures within and across different SLC gene subtypes. *SLC*, solute carrier; *RFS*, relapse-free survival; *OS*, overall survival; *CI*, confidence interval; *ADJC*, adjuvant chemotherapy; *R*, response; and *NR*, nonresponse.

sequence (Fig. 2A and B). The co-expression pattern of SLC family genes was also categorized into four clusters defined as SLC-C1, SLC-C2, SLC-C3, and SLC-C4 (Table S1). As shown in the heatmap (Fig. 2B) and boxplot (Fig. S4A), SLC-S1 and SLC-S2 were characterized by enrichment of the SLC family members in SLC-C3 and SLC-C4 clusters, respectively, suggesting that the substrate transmembrane transport process mediated by SLC-C3 and SLC-C4 was highly activated in the corresponding patients. Moreover, the average expression of the SLC genes contained in SLC-C1 was significantly elevated in the SLC-S3 and SLC-S5 subtypes, while the SLC members in the SLC-C2 cluster were mainly distributed in the SLC-S3 and SLC-S4 subtypes. Subsequent survival analysis demonstrated that (Fig. 2C) the RFS (recurrence-free survival) between five SLC subtypes was significantly different. Specifically, patients with SLC-S2 had the shortest RFS, whereas patients with SLC-S4 and SLC-S5 each had a better RFS than those with other SLC subtypes. As for overall survival (OS) (Fig. 2D–F), although we did not observe any statistical difference in OS between SLC subtypes ( $P = 0.082$ ) in the entire cohort, the correlation between SLC subtypes and OS was significant when subgroup analysis was stratified by adjuvant chemotherapy

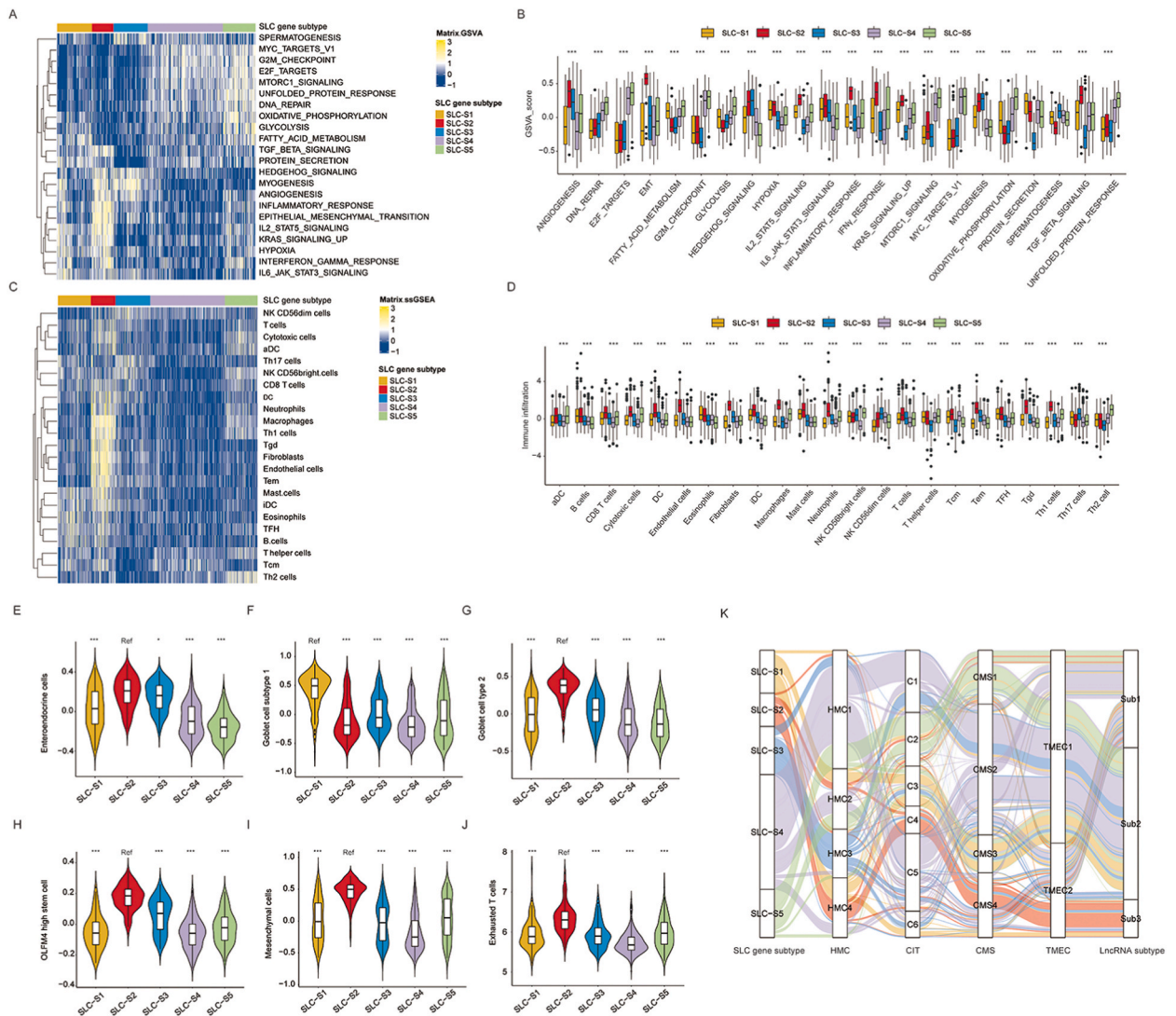


**Fig. 3.** Tumor microenvironment and biological function characteristics of distinct SLC gene subtypes. (A–B) Heatmap (A) and boxplot (B) show the biological pathway activation status based on “hallmark gene sets” in the five SLC gene subtypes in the *meta*-GEO cohort. Cohort details and SLC gene subtypes are used as sample annotations of the heatmaps. Boxes represent 25–75 % of values, lines in boxes represent median values, whiskers represent 1.5 interquartile ranges, and black dots represent outliers. (C–D) Heatmap (C) and box plot (D) illustrate the results of tumor microenvironment landscape in the five SLC gene subtypes in the *meta*-GEO cohort. Cohort details and SLC gene subtypes are used as sample annotations of the heatmaps. Boxes represent 25–75 % of values, lines in boxes represent median values, whiskers represent 1.5 interquartile ranges, and black dots represent outliers. (E–J) Violin plots of the abundance of the enteroendocrine cell (E), goblet cell subtype 1 (F), goblet cell subtype 2 (G), OLFM4 high stem cell (H), mesenchymal cell (I), and exhausted T cells (J) among five SLC gene subtypes in the *meta*-GEO. (K) Sankey diagram of SLC gene subtypes in groups with different molecular subtypes in the GSE39582 cohorts. <sup>#</sup> $p < 0.05$ , <sup>\*\*</sup> $p < 0.01$ , <sup>\*\*\*</sup> $p < 0.001$ ; ns, not significant; Ref, reference; SLC, solute carrier; HMC, histone modification cluster; CMS, consensus molecular subtypes; TMEC, tumor microenvironment cluster.

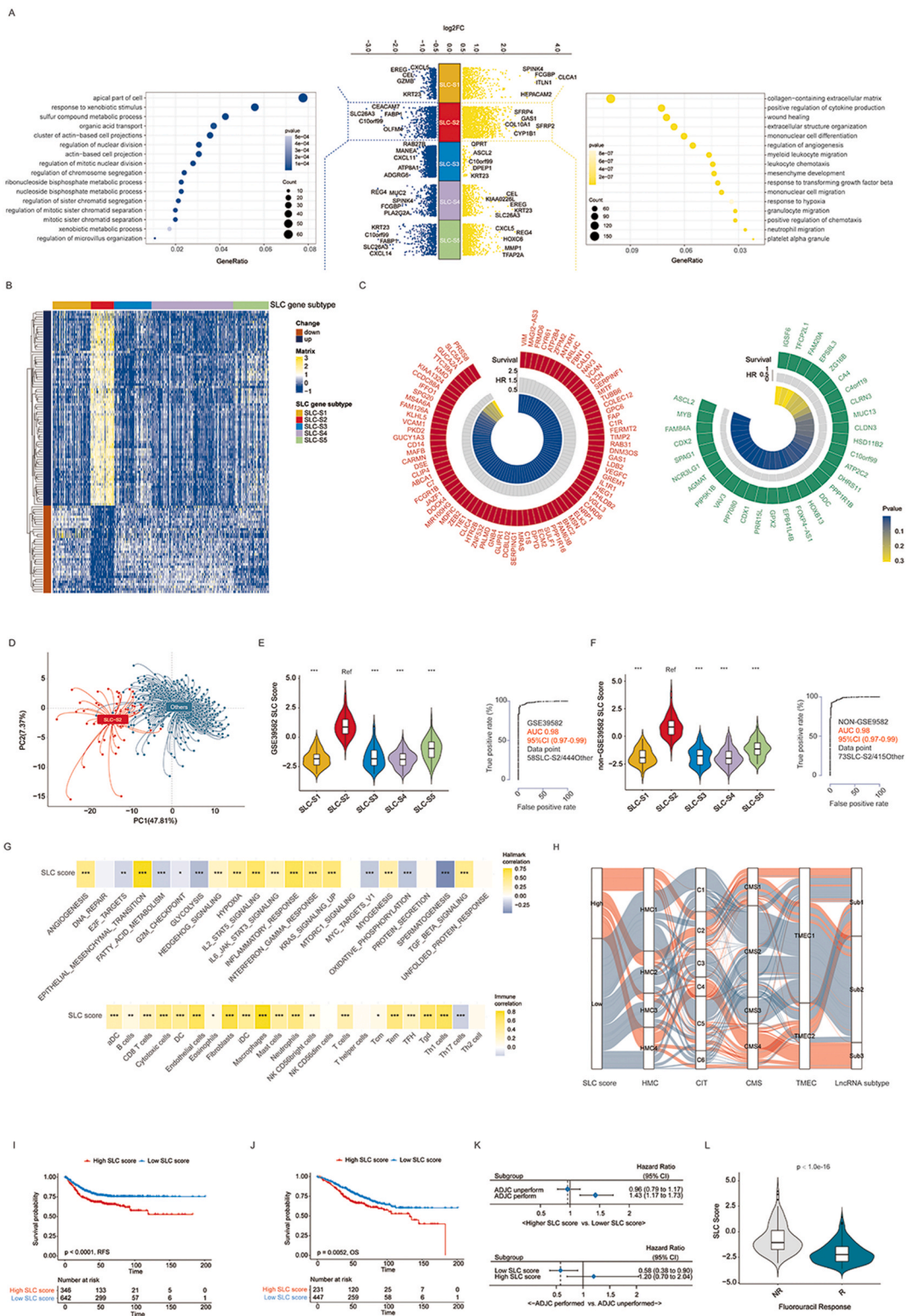
(ADJC) performance status. Particularly, in the subgroup without ADJC, SLC-S3 exhibited the worst prognosis (Fig. 2E), whereas SLC-S2 displayed the highest mortality risk in patients who received ADJC (Fig. 2F). These findings indicate that the SLC subtypes might be link to the benefit of ADJC in patients with colon cancer. To confirm this hypothesis, we further analyzed the survival benefits of ADJC among patients with distinct SLC subtypes. The forest plot (Fig. 2G) demonstrated that ADJC performance was associated with elevated mortality risk of SLC-S2 patients but provided survival benefits to non-SLC-S2 patients. Moreover, the matrix heatmap (Fig. 2H) and stacked histogram (Fig. 2I) illustrated that the fluorouracil response rate of patients with SLC-S2 was the lowest among all subtypes, whereas patients with SLC-S5 presented the highest fluorouracil response rate. Coincidentally, we noticed that the transcriptional expression of *SLC22A18*, a transporter belonging to the SLC22 family, was significantly reduced in the SLC-S2 compared to its expression in other SLC gene subtypes among the five tumor cell-enriched SLC transporters mentioned above (Fig. S5). Previous studies have also reported that the downregulated expression of *SLC22A18* could cause acquisition of oxaliplatin resistance among colon cancer cells [22] and temozolomide resistance in GBM U87 cells [23]. Given that SLC22 family members serve as drug uptake carriers with important roles in a wide range of pharmacological cancer therapies, including platinum-based drugs, taxanes, antimetabolites, and topoisomerase inhibitors [24], we speculated that a decrease in intracellular drug accumulation caused by low *SLC22A18* expression may be one of the mechanisms underlying chemoresistance in the SLC-S2 subtype. Collectively, these data illustrate that molecular classification based on the transcriptional profiling of SLC family genes could guide the clinical diagnosis and therapeutic strategies for patients with non-metastatic colon cancer.

To further confirm whether the association between different SLC subtypes and patient prognosis, as well as chemotherapy benefit, depended on the co-expression patterns of SLC gene clusters, we investigated the clinical relevance of the mean expression levels of SLC transporters in the four SLC gene clusters. The result illustrated that higher levels of SLC-C4 cluster expression were correlated with elevated relapse risk in all patients (Fig. S4B), increased mortality risk in the ADJC performed subgroup (Fig. S4C), and fluorouracil-nonresponse status (Fig. S4D). Conversely, the expression level of SLC-C2 exhibited significant positive correlation with the survival time of RFS in the total patients and of OS in the subgroups receiving ADJC (Figs. S4B–C). Moreover, the expression level of SLC-C1 was shown to be downregulated in the fluorouracil nonresponse group (Fig. S4D). Collectively, we believe that the co-expression patterns of SLC genes, specifically the overexpression of SLC-C4 combined with low abundance of SLC-C1 and SLC-C2, led to poor prognosis and fluorouracil resistance in patients with SLC-S2.

### 3.3. Biological and TME features among distinct SLC subtypes

To uncover the variation in biological pathway activation among the five SLC gene subtypes, we performed GSVA against the “Hallmark” gene set. As depicted in Fig. 3A and B, the activation levels of several items related to cell cycle regulation, including E2F signaling, G2M checkpoint, MTORC1 signaling, MYC signaling, DNA repair, and unfolded protein response, were significantly inhibited in SLC-S1, SLC-S2, and SLC-S3 subtypes, but they were highly augmented in SLC-S4 and SLC-S5 subtypes. Meanwhile, multiple pathways, including angiogenesis, EMT, IL-2-STAT5 signaling, IFN $\gamma$  response, KRAS signaling, and TGF- $\beta$  signaling, showed the highest GSVA scores in SLC-S2, suggesting that SLC-S2 may be characterized by the upregulation of stromal and immune inflammatory pathways. For the SLC-S3 subtype, aside from the cell cycle-related pathways mentioned above, the activation levels of KRAS signaling, protein secretion, and TGF- $\beta$  signaling pathways were also significantly downregulated in SLC-S3 cells compared to levels in the other subtypes. Interestingly, some metabolic pathways, such as oxidative phosphorylation, fatty acid metabolism, and glycolysis, were enriched to a certain degree in patients with SLC-S1, SLC-S4, and SLC-S5, indicating that inhibiting metabolism might be a viable therapeutic option for these patients.

Regarding the TME landscape of each SLC gene subtype (Fig. 3C and D), we found that, compared with other subtypes, the cell types contained in the TME of SLC-S2 tissue were the most abundant. The infiltration levels of various TME cells, including Tem, Tgd, Th1, macrophages, endothelial cells, fibroblasts, mast cells, and neutrophils, were significantly higher in SLC-S2 than in the other subtypes. We further confirmed that our previously developed SIIIS score, a scoring tool for measuring stromal components [13], was the highest in the SLC-S2 subtype (Fig. S6A). Therefore, we hypothesized that the TME feature of the SLC-S2 subtype may be identified as “immune-excluded”, which is featured by the infiltration of stromal cells resulting the sequestration of cytotoxic cells within the stroma encompassing tumor cell nests instead of infiltrating the tumor parenchyma [25]. SLC-S4 represented the “cold tumor” phenotype, with few cell types infiltrated. However, SLC-S1, SLC-S3, and SLC-S5 samples displayed moderate infiltration of several cell types, among which the SLC-S5 subtype was mainly infiltrated with cytotoxic cells. In addition to the cell type mentioned above, we also conducted deconvolution of the infiltration level of enteroendocrine cells (Fig. 3E), goblet cell subtype 1 (Fig. 3F), goblet cell subtype 2 (Fig. 3G), OLFM4<sup>+</sup> stem cells (Fig. 3H), mesenchymal cells (Fig. 3I), and T exhausted cells (Fig. 3J) from the transcriptomic profiles of the *meta*-GEO cohort based on the cell markers proposed in previous research [26]. The results indicated that all cells except goblet cell subtype 1 were enriched in the SLC-S2 subtype with the highest abundance, while the enrichment of goblet cell subtype 1 exhibited the highest level in SLC-S1 compared to the other subtypes. Subsequently, we explored the association between the SLC gene subtype and other reported molecular subtypes of colon cancer. As indicated in Fig. 3K, the SLC-S1 samples were mainly enriched in CMS3 [27], which displaying epithelial differentiation and strong upregulation of multiple metabolism signatures; while patients with SLC-S2 were mainly concentrated in HMC4 [14], C4 [28], CMS4 [27], TMEC2 [29] and Sub3 [30] subtypes, which represented stromal phenotypes. The majority of SLC-S3 samples were enriched in HMC3 [14], both of which share significant inhibition of the G2M checkpoint pathway. Furthermore, there was an overlap between SLC-S4, HMC1 [14], and CMS2 [27] subtypes, characterized by the activation of the MYC and WNT pathways. Finally, SLC-S5 patients were mostly concentrated in C2 [28] and CMS1 [27], both of which displayed immune infiltration and activation characteristics.



(caption on next page)

**Fig. 4.** Construction and exploration of the SLC score in the *meta*-GEO cohort. (A) The up (yellow)- and downregulated (blue) genes in all five SLC gene subtypes (middle). A gene ontology analysis depicted the enriched pathways of the genes downregulated (left) and upregulated (right) in patients in the SLC-S2 subtype. Circle size represents the number of genes enriched in this pathway. Circle color depth indicates *p* value. (B) Heatmap shows the expression of 133 genes consisting of SLC score in five SLC gene subtypes after dimension reduction using the Boruta algorithm. SLC gene subtypes are used as sample annotations of the heatmaps. (C) Circus plots showing the expression level and survival impact of 113 selected genes used for calculating SLC score (red, risk factor for relapse-free survival; green, protect factor for relapse-free survival). (D) Principal component analysis of 113 selected genes to distinguish SLC-S2 from other SLC gene subtypes. (E–F) Violin plot (left) of SLC score value in five SLC gene subtypes and receiver operating curve of SLC score (right) in the GSE39582 (E) and non GSE39582 samples (F) of the *meta*-GEO cohort. (G) The correlations of the SLC score with tumor microenvironment (lower) and biological pathway activation status (upper) in the *meta*-GEO cohort. (H) Sankey diagram of SLC score groups in groups with different molecular subtypes in the GSE39582 cohort. (I–J) Kaplan-Meier curves of relapse-free survival (I) and overall survival (J) in the *meta*-GEO cohort according to the SLC score. (K) Forest plot (upper) of associations between the SLC score and overall survival in subgroups stratified by adjuvant chemotherapy conduction in the GSE39582 cohort. Forest plot (down) of benefits of adjuvant chemotherapy in different SLC score groups in the GSE39582 cohort. (L) Violin plot of SLC score values among patients with different fluorouracil responses in the *meta*-GEO cohort. SLC, solute carrier; ADJC, adjuvant chemotherapy; RFS, relapse-free survival; OS, overall survival; CI, confidence interval; HMC, histone modification cluster; CMS, consensus molecular subtypes; TMEC, tumor microenvironment cluster; R, response; NR, nonresponse; and ADJC, adjuvant chemotherapy. (For interpretation of the references to color in this figure legend, the reader is referred to the Web version of this article.)

### 3.4. Construction and evaluation of SLC score in GEO cohorts

Because of the poor prognosis and low fluorouracil response rate in patients with SLC-S2, we believe that establishing a practical scoring model with the ability to accurately recognize such patients in clinical practice and assisting TNM staging to guide adjuvant chemotherapy strategies in colon cancer is necessary. For this purpose, we employed GSE39582 as the training cohort to identify the most informative genes for effectively distinguishing patients with SLC-S2. Based on the screening procedures and workflow depicted in Fig. S1, we started by recognizing DEGs in these five subtypes and identified 1003 DEGs in the SLC-S2 subtype (801 upregulated and 202 downregulated; Fig. 4A and Table S5). A gene ontology analysis of these DEGs demonstrated that the upregulated DEGs exhibited significant enrichment in biological processes associated with stromal activation, while the downregulated DEGs displayed enrichment in items pertaining to cell division and metabolic processes (Fig. 4A). Subsequently, based on the Boruta algorithm, we identified 113 genes to construct an SLC gene subtype-associated signature referred to “SLC score” (Fig. 4B and C). The expression levels of 81 genes were significantly increased in the SLC-S2 subtype, and their upregulated expression was significantly correlated with unfavorable prognosis. Conversely, the remaining 32 genes were markedly downregulated in patients with SLC-S2, and their downregulation displayed significant correlation with increased risk of relapse. Subsequent PCA revealed that genes comprising the SLC score were capable of effectively distinguishing patients with SLC-S2 from those with non-SLC-S2 subtypes (Fig. 4D). The boxplots (Fig. 4E and F, left) illustrate that the median value of SLC score was the highest in SLC-S2 subtype in both GSE39582 samples and other *meta*-GEO samples (validation cohort 1). The receiver operating characteristic (ROC, Fig. 4E and F, right) further illustrated that the SLC score was a reliable indicator for identifying SLC-S2 patients with a diagnostic accuracy of 0.98 in both the GSE39582 and non-GSE39582 cohorts. By conducting correlation tests (Fig. 4G and Fig. S6B), we discovered that the SLC score was significantly positively correlated with not only the activation degree of stromal relevant pathways but also the infiltration level of stromal cells, which was in accordance with the findings generated from the SLC-S2 subtype analysis. The enrichment of high- and low- SLC score group, which were defined by the “survminer” package, in previously documented molecular subtypes is shown in Fig. 4H.

Furthermore, we investigated the impact of SLC score on prediction of clinical outcomes for patients with colon cancer. The results indicated that the subgroup with low SLC score had notably higher RFS (hazard ratio [HR] = 1.64, 95% confidence interval [CI] = 1.28–2.12, Fig. 4I) and OS (HR = 1.47, 95%CI = 1.11–1.95, Fig. 4J). Further analysis of the SLC score as a continuous variable revealed that the SLC score served as an independent prognostic indicator for RFS (HR = 1.19, 95%CI = 1.08–1.32, Table S6). Moreover, as demonstrated in both univariate (HR = 1.45, 95%CI = 1.17–1.73, Fig. 4K, upper) and multivariate (HR = 1.44, 95%CI = 1.18–1.76, Table S6) analyses, the SLC score also showed a noteworthy correlation with OS in patients who underwent ADJC.

Regarding to the predictive value of the SLC score in assessing chemotherapeutic benefits, we recalibrated the cutoff value of SLC score according to ROC curve to examine the efficiency of the SLC score in identifying the SLC-S2 subtype. Consistent with our expectations, patients who could potentially benefit from ADJC were restricted to the low SLC score group (HR = 0.55, 95%CI = 0.38–0.90, Fig. 4K, lower). The violin plot further illustrated that the fluorouracil response group had significantly higher SLC scores than the non-responders (Fig. 4L). In conclusion, these findings demonstrated that the SLC score holds potential as a dependable biomarker for prognosticating prognosis and determining the chemotherapeutic benefits in patients diagnosed with colon cancer, thus exhibiting promising clinical transformation values.

### 3.5. Evaluation of SLC score in TCGA-COAD and SYSUCC cohorts

The performance of the SLC score was further estimated in the TCGA-COAD (validation cohort 2) and SYSUCC (validation cohort 3) cohorts. As shown in Fig. 5A, by utilizing the Submap algorithm, we confirmed that high SLC score patients shared significant similarity in transcriptome features with patients of the SLC-S2 subtype, while patients with low SLC scores shared distinct resemblance in transcriptome features with patients of the non-SLC-S2 subtype, indicating that the SLC score model could be applied to effectively identify patients with SLC-S2 in independent cohorts. Regarding the relationships between SLC score and the biological pathway

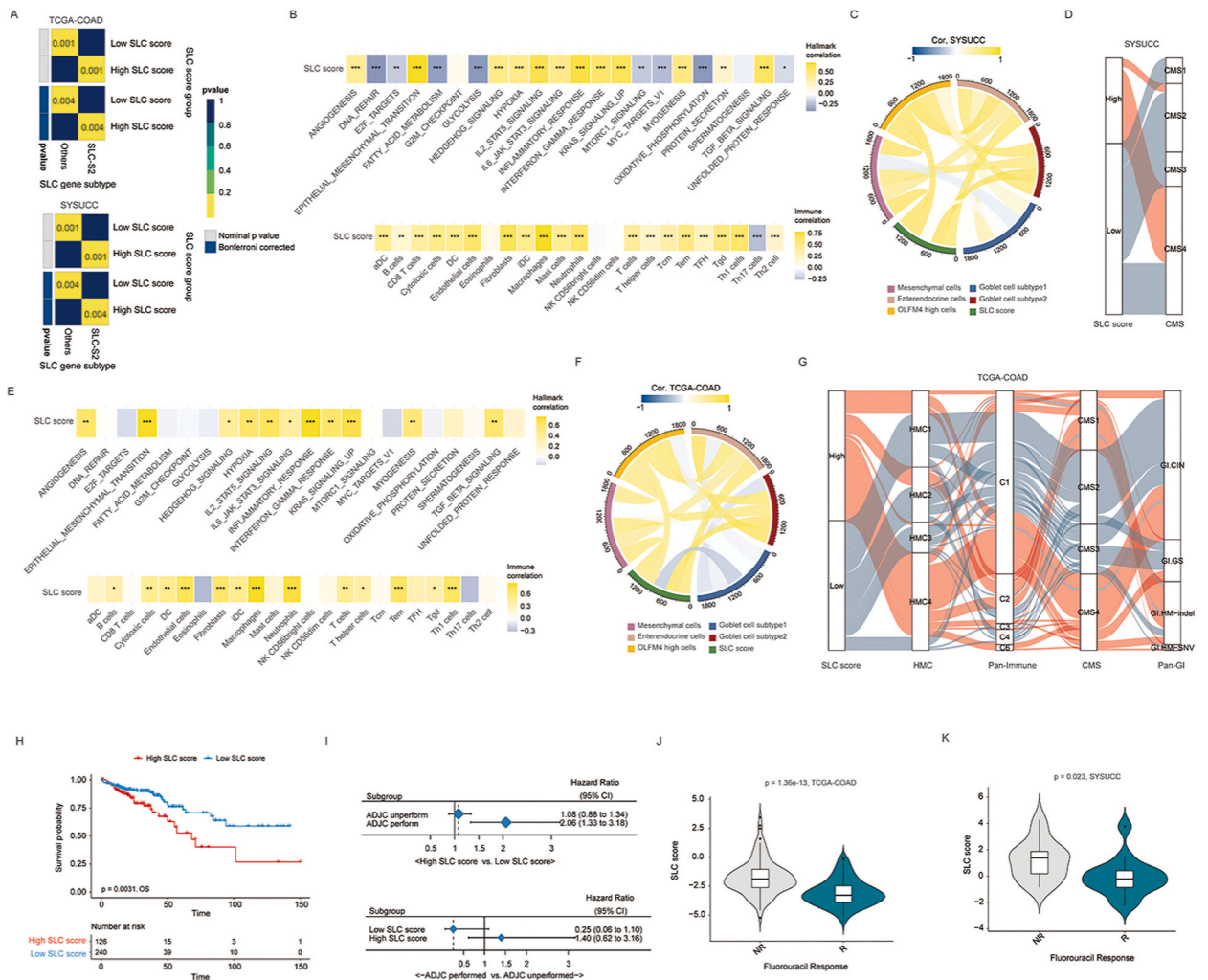


**Fig. 5.** Validation of the SLC score in the TCGA-COAD and SYSUCC cohort. (A) Heatmaps displaying the comparison of the transcriptome similarity between the SLC-S2 subtype in *meta*-GEO cohort and high SLC score group in TCGA-COAD (upper) and SYSUCC (down) cohorts. (B) The correlations of the SLC score with tumor microenvironment (lower) and biological pathway activation status (upper) in the SYSUCC cohort. (C) The correlation chord chart shows the mutual correlation between mesenchymal cell abundance, OLFM4 high cell abundance, secretory cell enrichment level, and SLC score in the SYSUCC cohort. (D) Sankey diagram of SLC score in different CMS subtypes in the SYSUCC cohort. (E) The correlations of the SLC score with tumor microenvironment (lower) and biological pathway activation status (upper) in the TCGA-COAD cohort. (F) The correlation chord chart shows the mutual correlation between mesenchymal cell abundance, OLFM4 high cell abundance, secretory cell enrichment level, and SLC score in the TCGA-COAD cohort. (G) Sankey diagram of SLC score in groups with different molecular subtypes in the TCGA-COAD cohort. (H) Kaplan–Meier curves of overall survival according to SLC score in the TCGA-COAD cohort. (I) Forest plot (upper) of associations between the SLC score and overall survival in subgroups stratified by adjuvant chemotherapy conduction of TCGA-COAD cohort. Forest plot (down) of benefits of adjuvant chemotherapy in different SLC score groups in the TCGA-COAD cohort. (J–K) Violin plot of SLC score values among patients with different fluorouracil responses in the TCGA-COAD (J) and SYSUCC (K) cohort. \* $p < 0.05$ , \*\* $p < 0.01$ , \*\*\* $p < 0.001$ . SLC, solute carrier; ADJC, adjuvant chemotherapy; RFS, relapse-free survival; OS, overall survival; CI, confidence interval; HMC, histone modification cluster; CMS, consensus molecular subtypes; TMEC, tumor microenvironment cluster; R, response; NR, nonresponse; and ADJC, adjuvant chemotherapy.

activation as well as TME cell infiltration, a significant positive correlation was observed between the SLC score and various factors including the activation level of stromal and inflammatory pathways, SIIS value, abundance of stromal cells, enteroendocrine cells, goblet cell subtype 2, OLFM4<sup>+</sup> stem cells, and mesenchymal cells in both SYSUCC (Fig. 5B–C and Fig. S6C) and TCGA-COAD (Fig. 5E–F and Fig. S6D) cohorts. Additionally, the enrichment of high SLC score groups in the CMS4 subtype was evident in both cohorts (Fig. 5D and G). These findings were aligned with the results obtained from *meta*-GEO cohort.

In terms of clinical relevance, in the TCGA-COAD cohorts, the mortality rate of patients with elevated SLC scores exhibited a significant increase compared to those with lower SLC scores (HR = 2.04, 95 % CI = 1.27–3.32, Fig. 5H). Moreover, the SLC score exhibited a significant correlation with OS in both univariate (HR = 2.06, 95 % CI = 1.33–3.18, Fig. 5I, upper) and multivariate (HR = 2.13, 95 % CI = 1.36–3.33, Table S7) Cox regression as a continuous variable in the subgroup that received ADJC. Further analysis of

chemoresponses illustrated that patients with high SLC score were also unable to benefit from ADJC (HR = 1.40, 95 % CI = 0.62–3.16, Fig. 5I, bottom), and the fluorouracil non-response group was characterized by markedly higher SLC scores than those of the fluorouracil response group in the TCGA-COAD (Fig. 5J) and SYSUCC (Fig. 5K) cohorts. These findings indicate strong reproducibility of the SLC score to predict prognosis and chemotherapy efficacy in patients with colon cancer.

### 3.6. The multi-omics analysis of samples in different SLC score groups

In order to enhance the understanding of the biological characteristics between different SLC score groups, a multi-omics analysis was carried out within the TCGA-COAD cohort. First, as for the distribution of CNV events, we found that the chromosomal aberrations between the high- and low SLC score group were similar (Fig. 6A and B). By using Chi-square test, we identified 11 altered (amplifications or deletions) copy number events, the frequency of which was significantly higher in the low SLC score group compared to that of the high score group (adj p-value < 0.05, Fig. 6C), and these copy number events were located on chromosome 20 (5 events), chromosome 18 (5 events) and chromosome 17 (1 event) respectively. In terms of somatic mutations (Fig. 6D), we identified that the mutation rates of 10 SMGs, including *BRAF*, *RNF43* and several other genes, were significantly different between high and low SLC score groups of patients, and the mutation rates of these SMGs were significantly enriched in the high subgroup. Although the mutation

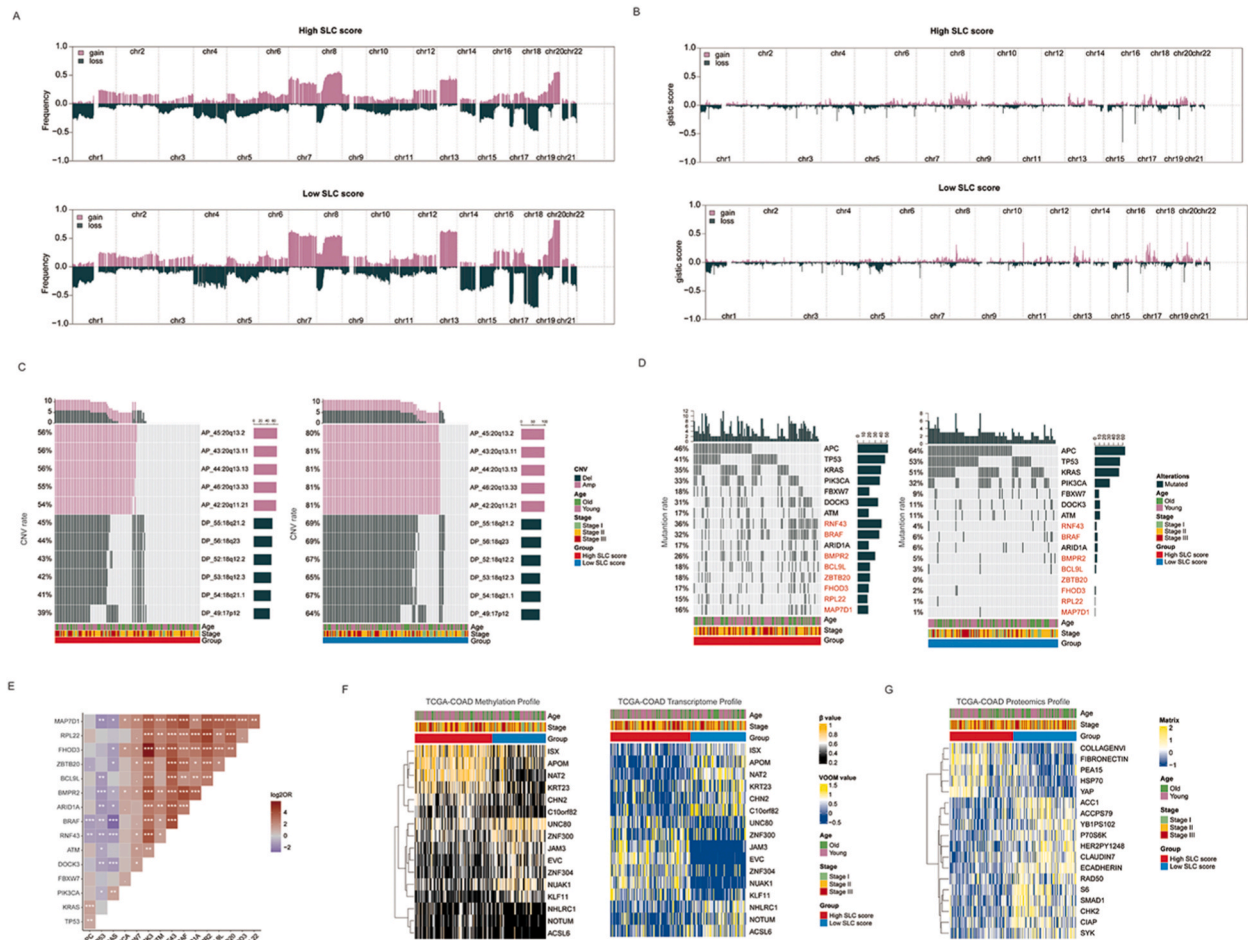


**Fig. 6.** SLC score-related multi-omics characteristics Composite copy number profiles for high SLC score and low SLC score tumours with gains in purple and losses in dark green. (B) Distribution of gistic score in high SLC score and low SLC score tumours with gains in purple and losses in dark green. (C) Oncoprints Oncoplot displays most frequently altered (amplifications or deletions) copy number events ordered according to the frequency. Cohort details and SLC score groups are used as sample annotations of the heatmaps. (D) Oncoprints depicted the somatic mutations of significant mutated genes in the context of high SLC score and low SLC score tumours. Cohort details and SLC score groups are used as sample annotations of the heatmaps. (E) Heatmap for genes with mutual exclusivity or co-occurrence. Stars refer to correlations that are statistically significant. (F) Heatmaps of significantly varied methylation genes in high SLC score and low SLC score tumours at methylation level (left) and transcriptome level (right). (G) Heatmap exhibited the landscape of differentially expressed proteins in five SLC subtypes. \* $p < 0.05$ , \*\* $p < 0.01$ , \*\*\* $p < 0.001$ ; CNV, copy number variations; Del, deletion; Amp, amplification; OR, odds ratio. (For interpretation of the references to color in this figure legend, the reader is referred to the Web version of this article.)

rates of *APC* and *KRAS* exhibited significant increase in the low SLC score subgroup, the significance was lost after Bonferroni correction. The co-occurrence status of these genes was shown in Fig. 6E. Aside from genomic mutations, we compared the disparities in gene promoter methylation levels between high and low SLC score groups. As shown in Fig. 6F and 16 SVMGs have been recognized. Among these genes, nine SVMGs demonstrated low transcriptional expression accompanied by high methylation levels, whereas the remaining genes exhibited high transcriptional expression along with low methylation levels in the high score group. The overall methylation levels of the *NHLRC1*, *NOTUM*, and *ACSL6* genes were all low. Finally, by analyzing the proteomic data from the TCGA-COAD cohorts (Fig. 6G), we found that samples with high SLC scores had significant overexpression of proteins implicated in EMT and TGF- $\beta$  signaling, which further verified the transcriptomic GSEA results at the protein level.

### 3.7. The correlation between the SLC gene subtype, SLC score, and the immunotherapy response

Previous research has reported that patients with an “immune-excluded” phenotype exhibited low response rates towards PD-L1 blockade [31]. Considering that the TME infiltration features of both SLC-S2 and high-SLC score patients were characterized by the enrichment of stromal cells, we sought to find out whether the SLC gene subtype and SLC score were correlated with the immunotherapeutic response probability. Here, the TIDE algorithm was employed to forecast the likelihood of immunotherapy response. We found that patients with SLC-S2 had a lower likelihood of responding to immunotherapy compared to other SLC gene subtypes, which were characterized by the highest nonresponsive rates in meta-GEO cohorts (Fig. 7A). Similarly, in the meta-GEO and TCGA-COAD cohorts, the SLC score exhibited a significant increase among the predicted immunotherapy non-responders (Fig. 7B) and was strongly positively associated with the TIDE score (Fig. 7C). However, although the SLC score demonstrated a positive correlation with the TIDE score in the SYSUCC cohort, no statistical differences were observed ( $P = 0.094$ , Fig. 7C). Aside from TIDE prediction, the Submap algorithm was utilized to compare the transcriptional profiling of the SLC gene subtypes with the published pretreatment transcriptomic data of 217 metastatic urothelial cancer patients who received anti-PD-L1 therapy. The results demonstrated that patients of the SLC-S2 (Fig. 7D, upper) and the high-SLC score groups (Fig. 7D, bottom) exhibited significant resemblance in transcriptional features with the nonresponsive patients to anti-PD-L1 therapy, which further indicated that the SLC-S2 subtype and patients with high SLC scores may not be candidates that could benefit from anti-PD-1 treatment (adjusted  $P = 0.008$ ).

### 3.8. Potential compounds for chemosensitization in colon cancer patients with high SLC scores

We attempted to explore potential compounds that may be applied as chemosensitizers for patients with high SLC scores. By employing CTRP data to explore whether the AUC of compounds correlates with the SLC score, we discovered 24 compounds with correlation coefficients less than  $-0.5$  (Fig. 8A) in the GSE39582, TCGA-COAD, and SYSUCC cohorts (Tables S8–S10). Further investigation of the activities and gene targets of these compounds revealed that the five compounds of them were the inhibitors of PI3K catalytic subunit family (Fig. 8B and C). Among them, XK765 and PI-103 exhibited targeting capabilities towards various catalytic subunits of PI3K; the AZD6482 and TGX-221 demonstrated inhibitory effects on the activity of PIK3CB, while CAL-101,

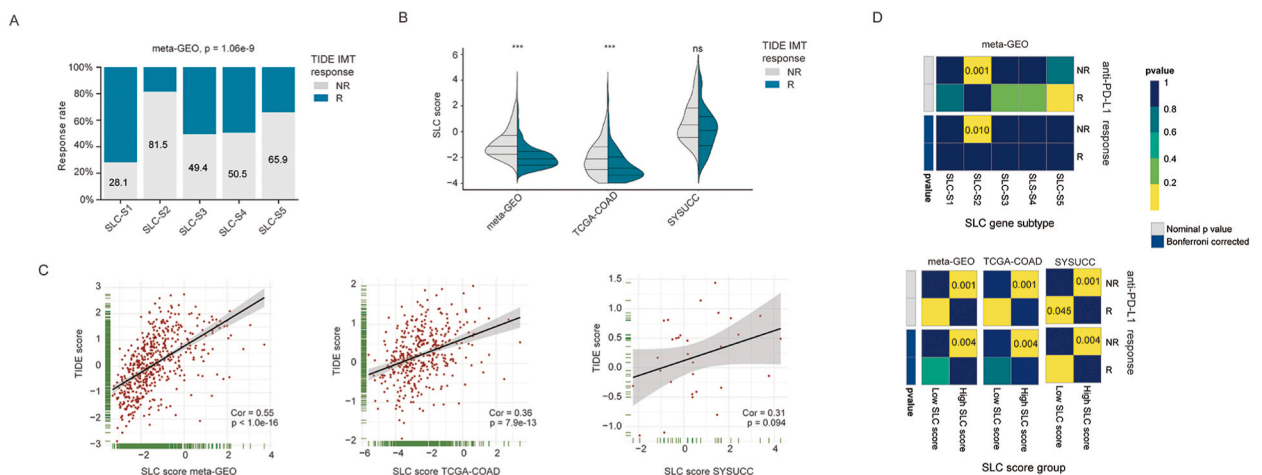


**Fig. 7.** The associations between SLC score and immunotherapy benefits. (A) Bar charts summarizing the proportions of patients with immunotherapy response and those with nonresponse predicted by TIDE algorithm within and across SLC gene subtypes in the GSE39582. (B) Violin plot of SLC score values in immunotherapy response and nonresponse groups predicted by TIDE algorithm in GSE39582, TCGA-COAD, and SYSUCC cohorts. (C) Scatter plots showing the correlations between SLC score value and TIDE score in the GSE39582, TCGA-COAD, and SYSUCC cohorts. (D) Heatmap (upper) showing the comparison of the similarity between SLC gene subtypes and immunotherapy response of IMvigor210 dataset in GSE39582 cohort revealed by SubMap analysis. Heatmap (below) displaying the comparison of the similarity between SLC score group and immunotherapy response of IMvigor210 dataset in GEO, TCGA-COAD, and SYSUCC. *SLC*, solute carrier; *TIDE*, tumor immune dysfunction and exclusion; *R*, response; and *NR*, nonresponse.

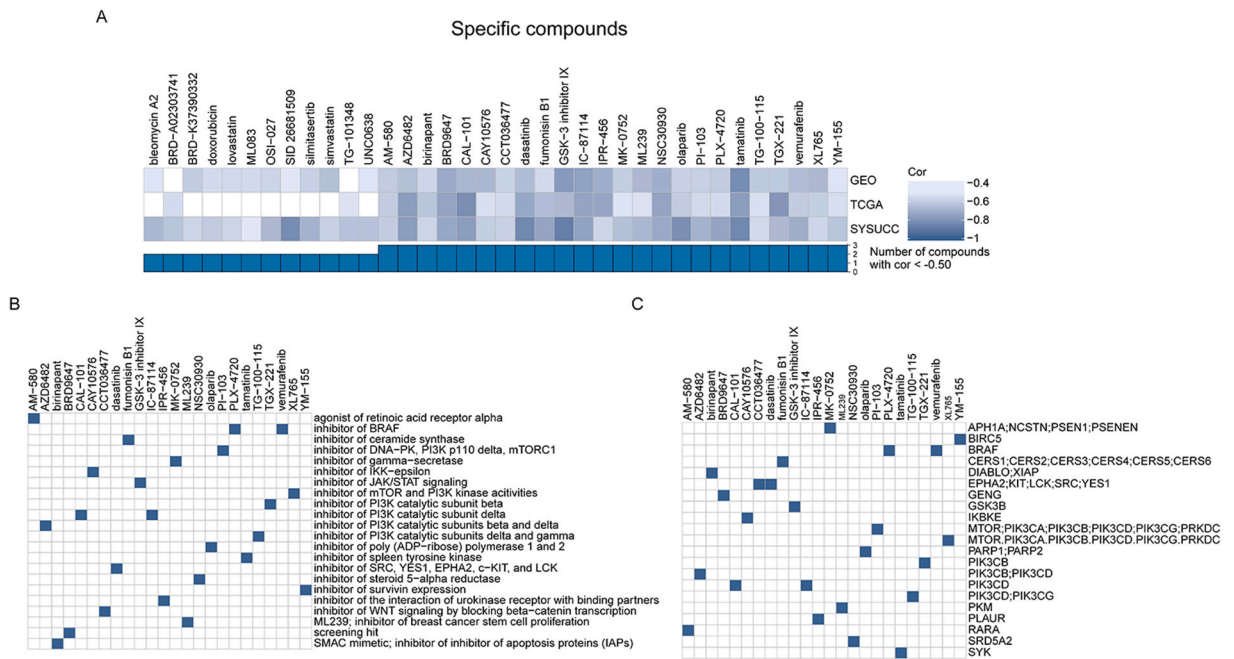


**Fig. 8.** Screening of candidate compounds for chemosensitization (A) Heatmaps showing the correlation between SLC score and predicted AUC of compounds based on CTRP database analysis. (B) Heatmap showing the mechanisms of the action (left) and gene targets (right) and of compound. *SLC*, solute carrier; *R*, response; *NR*, nonresponse; and *ADJC*, adjuvant chemotherapy.

AZD6482, TG-100-115, and IC-87114 exhibited inhibitory effects on the activity of PIK3CD. These results offer a novel outlook for developing efficacious chemosensitizing therapeutic approaches for colon cancer patients with high SLC scores.

#### 4. Discussion

SLC transporters exert many crucial physiological functions, including nutrient absorption, ion import/export, toxin metabolism, and waste clearance, and they have been implicated in the initiation and progression of many diseases [1,2]. However, as a largely understudied superfamily, the role of many SLCs remains unclear, especially in the initiation and progression of human malignancy. Moreover, whether SLC transporters can be employed as biomarkers for cancer diagnosis and prediction of prognosis and therapeutic outcome remains to be explored. The intestinal tract is regarded as the most critical organ in the communication and interaction with exogenous substances like food and chemicals; therefore, SLC transporters also act as critical participants in maintaining intestinal cellular homeostasis, and the dysregulation of SLC transporters may be robustly associated with the progression of colon cancer [32]. In this study, by utilizing scRNA-seq data of colon cancer to compare the expression differences of SLC transporters between tumor cells and non-cancerous cells, we noticed that some SLC transporters tend to be expressed in a cell-type propensity manner, and five of them were defined as tumor cell-enriched SLC transporters because they were highly expressed in tumor cells and nearly absent in all types of non-tumor cells. Among these tumor cell-enriched SLC transporters, *SLC2A1* was the most unique, as only high expression of *SLC2A1* was significantly associated with worse RFS and worse OS in both the ADJC-performed and ADJC-unperformed subgroups. *SLC2A1* belongs to the SLC2A family, which is primarily responsible for glucose transportation, and has been reported to act as master activators to reprogram cancer metabolism, thereby promoting tumor progression [33–35]. Based on our analysis results, we propose that *SLC2A1* has potential as a molecular target for developing precise therapeutic strategies targeting tumor cell metabolism. Interestingly, we also found that another member of the SLC2 family, *SLC2A3*, was predominantly expressed in various immune cells except for plasma cells but lost its expression in tumor cells. Previous studies have demonstrated that glucose metabolism variation is not limited to different tumor cells but also occurs in various non-cancerous cellular components, including T cells, macrophages, cancer-associated fibroblasts, and endothelial cells [6,7]. Therefore, combined with the results of scRNA-seq data analysis, we think that it is more important to focus on the oncogenic effect of *SLC2A3* in the formation of TME features by regulating the metabolism of glucose in non-cells rather than its direct effect on tumor cells.

Previous studies comparing healthy and cancerous cells illustrated that SLC proteins have more pronounced alterations in their co-expression networks than those of protein kinases [1]. Meanwhile, the cellular absorption and excretion of various biomolecules are modulated under the strict monitoring of a specified network of SLC transporters [1,2]. Therefore, in this context, two issues aroused our concern: the specific co-expression pattern of different SLC transporters in colon cancer and whether their co-expression pattern contributes to patients' stratification or influences the clinical features of colon cancer. To answer these questions, we performed the unsupervised consensus clustering utilizing the transcriptomic data of 187 SLC family genes in the *meta*-GEO cohort. Our results

demonstrated that the SLC transporters comprised four distinct co-expression clusters, with each cluster containing dozens of SLC transporters affiliated to different subfamilies, which were responsible for transporting a diverse array of substrates. Based on the discrepant combination modes of these co-expression clusters, patients with colon cancer were further divided into five molecular subtypes that correlated with distinct clinical outcomes, biological pathways, and TME features. Among the five SLC gene subtypes, both the SLC-S1 and SLC-S2 subtypes were enriched by a single co-expression cluster, whereas the SLC-S3, SLC-S4, and SLC-S5 subtypes were characterized by moderate to high expression of more than one cluster. The results presented above imply that the heterogeneous progression of colon cancer is triggered by SLC transporters in a highly coordinated manner, which indicates that it is insufficient for researchers to target a single SLC gene when exploring the molecular biological functions of SLC family genes in tumor initiation and progression. Therefore, investigating the interaction among multiple SLC transporters from a comprehensive perspective is necessary. Our research provides a foundation for further exploration of the interplay between the diverse SLC family molecules underlying tumor development in colon cancer; in other words, SLC transporters belonging to the same cluster are presumably synergistically involved in substrate translocation and subsequent metabolic processes.

Among the five SLC gene subtypes, SLC-S2 stood out as the most crucial one. Patients within this subtype had the highest relapse risk and could not experience any advantages from fluorouracil-based ADJC due to their poor response to fluorouracil. In the meantime, individuals diagnosed with SLC-S2 exhibited a diminished probability of responding to immune checkpoint blockade therapy, as anticipated by the TIDE algorithm and SubMap analysis based on the transcriptional traits of the SLC-S2 patients. Furthermore, when compared to other subtypes, the SLC-S2 subtype exhibited extensive infiltration of stromal and myeloid cells, along with significant activation of numerous stromal-related pathways. Such stroma-dominated TME mode have been validated as crucial elements contributing to unfavorable chemotherapy and immunotherapy outcomes, as stated in prior studies [13,29–31]. Thus, in consideration of the special clinical features of patients with the SLC-S2 subtype, an SLC score model was developed and verified. This model was calculated by the transcriptional expression level of 113 protein-coding genes and able to accurately identify SLC-S2 patients or patients whose transcriptional characteristics are close to the SLC-S2 subtype in several independent cohorts. This finding also verified that the aberrant transcriptomic upregulation of oncogenes or, conversely, the repression of tumor suppressors is involved in the upstream and downstream regulation of aberrantly expressed SLC family genes [24]. Clinical analyses further highlighted that the SLC score independently predicts the prognosis of colon cancer and correlates with responses to chemotherapy and immunotherapy. Collectively, these findings demonstrated that the clinical transformation potential of the co-expression pattern of SLC transporters could be achieved by the SLC score, which exhibits outstanding reproducibility and clinical applicability to guide therapeutic strategies. It is worth noting that in somatic genomic mutation analysis, we discovered that the BRAF mutation, a marker for highly aggressive disease phenotype [36], was significantly enriched in high SLC score patients, suggesting that BRAF pathway activation may be one of the molecular mechanisms leading to adverse clinical outcomes in such a patient group.

To date, as their accumulating functions have been annotated, researchers are increasingly interested in developing tumor therapeutic drugs that target SLC transporters. Several *in vitro* and *in vivo* researches have corroborated the notion that some SLC inhibitors, including JPH203 [37], AZD3965 [38], and  $\gamma$ -glutamyl-*p*-nitroanilide [39], hamper tumor growth and metastasis as well as sensitize tumor cells to other chemotherapeutic agents by disrupting the metabolic homeostasis of tumor cells. Unfortunately, none of these drugs have been successfully validated in the clinical setting. Meanwhile, exploitation of SLC transporters as targets for development of anticancer drugs is difficult to achieve owing to many obstacles encountered in clarifying the structural characterizations of SLC transporters [40]. Therefore, although our data analysis suggests that SLC2A1 may be an ideal target for anti-tumor therapy, we also explored the associations between the AUC value of existing small compounds involved in the CTRP database and the SLC score value to screen for potential compounds suitable for enhancing chemosensitivity in SLC-S2 patients. Intriguingly, we noticed several compounds targeting PI3K catalytic subunits, the AUC values of which exhibited significant negative correlation with SLC scores in the three cohorts. Current research has demonstrated a strong relationship between the PI3K/AKT pathway and the SLC family of molecules, where they usually function as downstream of SLC transporters in a variety of biological processes [41,42]. Moreover, the RNF43 mutation, which is enriched in the high-SLC score group, has been confirmed as an oncogenic colorectal cancer mutation that sensitizes tumor cells to PI3K/mTOR inhibition [43]. Therefore, although further preclinical investigations *in vivo* and *in vitro* are needed, we postulate that PI3K inhibitors are likely to become potential efficacious candidates for guiding therapeutic strategies of patients with high SLC scores. Moreover, these findings also shed light on solving the technical problem that SLC transporters face difficulties when used as specific anti-cancer targets.

This research had several limitations. First, our analysis did not encompass all 456 SLC family genes. This is partly because the transcriptome profiles of *meta*-GEO and TCGA-COAD cohorts did not cover the complete SLC families. Moreover, our data cleaning strategy allowed SLC genes with low transcriptional expression abundance to be excluded. Although elimination of low-expressed genes is a common strategy used in bioinformatics analysis to make results more robust, it may inevitably exclude some SLC transporters that possess crucial pathophysiological roles and clinical relevance (e.g., SLC families responsible for anticancer drug cell accumulation). Second, the potential link between the expression of tumor cell-enriched SLC transporters and the development/progression of colorectal cancer revealed by our study requires further experimental verification. Next, the exploration and validation of the performance of the SLC score in prognosticating survival and therapeutic outcomes in colon cancer were only carried out in retrospective databases, which should be further verified. Finally, the cut-off values of the SLC score should be standardized in future prospective studies.

## 5. Conclusions

In conclusion, our study established a novel molecular subtype system for colon cancer, which not only systematically revealed the

complex interaction patterns among the SLC family molecules, but also reflected tumor heterogeneity related to the clinical behavior, TME, and biological behavior of colon cancer, providing new insights into colon cancer treatment. Developing a deeper understanding regarding the structure, function, expression, and regulation of SLC transporters may contribute to establishing definitive roles for SLC transporters and exploring novel targets and agents for cancer treatment. Moreover, we propose the SLC score as a reliable tool for identifying distinct SLC gene subtypes, thus providing more precise therapeutic guidance for the treatment of colon cancer.

### Ethics statement

This study was approved by the Human Research Ethics Committee of Nanfang Hospital (NFEC-2019-263) and was conducted according to the principles of the Declaration of Helsinki.

### Consent for publication

Not applicable.

### Funding sources

This work was supported by the National Natural Science Foundation of China (No. 82102731 to RZ, No. 82073303 to WL), Natural Science Foundation of Guangdong Province of China (2020A1515110686 to RZ, 2022A1515012418 to RZ), President Foundation of Nanfang Hospital, Southern Medical University (2020C020 to RZ).

### Contributor information

Wangjun Liao: [nfyyliaowj@163.com](mailto:nfyyliaowj@163.com).

### Data availability statement

The public data used in this study are available at:

GSE17536 (<http://www.ncbi.nlm.nih.gov/geo/query/acc.cgi?acc=GSE17536>); GSE33113 (<http://www.ncbi.nlm.nih.gov/geo/query/acc.cgi?acc=GSE33113>); GSE37892 (<http://www.ncbi.nlm.nih.gov/geo/query/acc.cgi?acc=GSE37892>); GSE38832 (<http://www.ncbi.nlm.nih.gov/geo/query/acc.cgi?acc=GSE38832>); GSE39582 (<http://www.ncbi.nlm.nih.gov/geo/query/acc.cgi?acc=GSE39582>);

GSE188711 (<http://www.ncbi.nlm.nih.gov/geo/query/acc.cgi?acc=GSE188711>);

TCGA-COAD (<https://xenabrowser.net/datapages/?cohort=TCGA> Colon Cancer (COAD); IMvigor210 R package "IMvigor210CoreBiologies".

The SUSYCC colon cancer dataset generated and analyzed during the current study are not publicly available but are available from the corresponding author on reasonable request.

### CRedit authorship contribution statement

**Rui Zhou:** Conceptualization, Data curation, Formal analysis, Funding acquisition, Writing – original draft, Writing – review & editing. **Lingbo Li:** Data curation, Formal analysis, Visualization, Writing – original draft, Writing – review & editing. **Yue Zhang:** Data curation, Visualization, Writing – original draft, Writing – review & editing, Formal analysis. **Zhihong Liu:** Validation, Visualization, Writing – review & editing. **Jianhua Wu:** Validation, Visualization, Writing – review & editing. **Dongqiang Zeng:** Visualization, Writing – review & editing. **Huiying Sun:** Validation, Writing – review & editing. **Wangjun Liao:** Conceptualization, Funding acquisition, Project administration, Supervision, Validation, Writing – review & editing.

### Declaration of competing interest

The authors declare that they have no known competing financial interests or personal relationships that could have appeared to influence the work reported in this paper.

### Acknowledgements

We would like to thank TCGA and GEO databases for their contribution.

### Abbreviations

AJDC    adjuvant chemotherapy  
CI       confidence interval  
CMS     consensus molecular subtypes

CNV	copy number variation
COAD	colon adenocarcinoma
CTRP	Cancer Therapeutics Response Portal
DEGs	deferentially expressed genes
EMT	epithelial-mesenchymal transition
FC	fold change
GEO	Gene Expression Omnibus
HMC	histone modification cluster
ICB	immune checkpoint blockade
ITH	intratumoral heterogeneity
MT	mutant type
NEO	neoantigen
NR	nonresponse
OS	overall survival
R	response
Ref	reference
RFS	relapse-free survival
ROC	receiver operating characteristic
SLC	solute carrier
SIIS	stromal infiltration intensity score
SMG	significant mutated gene
SVMG	significantly varied methylation gene
SYSUCC	Sun Yat-sen University Cancer Center
TCGA	The Cancer Genome Atlas
TIDE	tumor immune dysfunction and exclusion
TMB	tumor mutation burden
TME	tumor microenvironment
UCSC	University of California Santa
WT	wild type

## Appendix A. Supplementary data

Supplementary data to this article can be found online at <https://doi.org/10.1016/j.heliyon.2023.e22775>.

## References

- [1] A. Cesar-Razquin, B. Snijder, T. Frappier-Brinton, R. Isserlin, G. Gyimesi, X. Bai, R.A. Reithmeier, D. Hepworth, M.A. Hediger, A.M. Edwards, G. Superti-Furga, *Cell* 162 (2015) 478–487.
- [2] L. Lin, S.W. Yee, R.B. Kim, K.M. Giacomini, *Nat. Rev. Drug Discov.* 14 (2015) 543–560.
- [3] Y. Jung, Y. Jun, H.Y. Lee, S. Kim, Y. Jung, J. Keum, Y.S. Lee, Y.B. Cho, S. Lee, J. Kim, *Oncotarget* 6 (2015) 25368–25380.
- [4] K. Rashid, A. Ahmad, L. Liang, M. Liu, Y. Cui, T. Liu, *Drug Discov. Today* 26 (2021) 1689–1701.
- [5] C.C. Wong, Y. Qian, X. Li, J. Xu, W. Kang, J.H. Tong, K.F. To, Y. Jin, W. Li, H. Chen, M.Y. Go, J.L. Wu, K.W. Cheng, S.S. Ng, J.J. Sung, Z. Cai, J. Yu, *Gastroenterology* 151 (2016) 945–960 e946.
- [6] R. Chen, L. Chen, *Trends Cell Biol.* 32 (2022) 186–201.
- [7] W. Song, D. Li, L. Tao, Q. Luo, L. Chen, *Acta Pharm. Sin.* B 10 (2020) 61–78.
- [8] H. Sung, J. Ferlay, R.L. Siegel, M. Laversanne, I. Soerjomataram, A. Jemal, F. Bray, *Ca, Cancer J. Clin.* 71 (2021) 209–249.
- [9] W. Wang, R. Kandimalla, H. Huang, L. Zhu, Y. Li, F. Gao, A. Goel, X. Wang, *Semin. Cancer Biol.* 55 (2019) 37–52.
- [10] T. Reinert, T.V. Henriksen, E. Christensen, S. Sharma, R. Salari, H. Sethi, M. Knudsen, I. Nordentoft, H.T. Wu, A.S. Tin, M. Heilskov Rasmussen, S. Vang, S. Shchegrova, A. Frydendahl Boll Johansen, R. Srinivasan, Z. Assaf, M. Balcioglu, A. Olson, S. Dashner, D. Hafez, S. Navarro, S. Goel, M. Rabinowitz, P. Billings, S. Sigurjonsson, L. Dyrskjot, R. Swenerton, A. Aleshin, S. Laurberg, A. Husted Madsen, A.S. Kannerup, K. Stribolt, S. Palmelund Krag, L.H. Iversen, K. Gotschalck Sunesen, C.J. Lin, B.G. Zimmermann, C. Lindbjerg Andersen, *JAMA Oncol.* 5 (2019) 1124–1131.
- [11] J. Tie, J.D. Cohen, K. Lahouel, S.N. Lo, Y. Wang, S. Kosmider, R. Wong, J. Shapiro, M. Lee, S. Harris, A. Khattak, M. Burge, M. Harris, J. Lynam, L. Nott, F. Day, T. Hayes, S.A. McLachlan, B. Lee, J. Ptak, N. Silliman, L. Dobbyn, M. Popoli, R. Hruban, A.M. Lennon, N. Papadopoulos, K.W. Kinzler, B. Vogelstein, C. Tomasetti, P. Gibbs, D. Investigators, *N. Engl. J. Med.* 386 (2022) 2261–2272.
- [12] Y. Wang, L. Li, J.D. Cohen, I. Kinde, J. Ptak, M. Popoli, J. Schaefer, N. Silliman, L. Dobbyn, J. Tie, P. Gibbs, C. Tomasetti, K.W. Kinzler, N. Papadopoulos, B. Vogelstein, L. Olsson, *JAMA Oncol.* 5 (2019) 1118–1123.
- [13] R. Zhou, Z. Wen, Y. Liao, J. Wu, S. Xi, D. Zeng, H. Sun, J. Wu, M. Shi, J. Bin, Y. Liao, W. Liao, *Comput. Struct. Biotechnol. J.* 20 (2022) 2153–2168.
- [14] R. Zhou, F. Xie, K. Liu, X. Zhou, X. Chen, J. Chen, S. Xi, Z. Huang, X. Rong, *Clin. Epigenet.* 14 (2022) 70.
- [15] W. Guo, C. Zhang, X. Wang, D. Dou, D. Chen, J. Li, *JCI insight* 7 (2022).
- [16] L. Zhang, Z. Li, K.M. Skrzypczynska, Q. Fang, W. Zhang, S.A. O'Brien, Y. He, L. Wang, Q. Zhang, A. Kim, R. Gao, J. Orf, T. Wang, D. Sawant, J. Kang, D. Bhatt, D. Lu, C.M. Li, A.S. Rapaport, K. Perez, Y. Ye, S. Wang, X. Hu, X. Ren, W. Ouyang, Z. Shen, J.G. Egen, Z. Zhang, X. Yu, *Cell* 181 (2020) 442–459 e429.
- [17] E. Becht, N.A. Giraldo, L. Lacroix, B. Buttard, N. Elarouci, F. Petitprez, J. Selves, P. Laurent-Puig, C. Sautes-Fridman, W.H. Fridman, A. de Reynies, *Genome Biol.* 17 (2016) 218.
- [18] G. Bindea, B. Mlecnik, M. Tosolini, A. Kirilovsky, M. Waldner, A.C. Obenaus, H. Angell, T. Fredriksen, L. Lafontaine, A. Berger, P. Bruneval, W.H. Fridman, C. Becker, F. Pages, M.R. Speicher, Z. Trajanoski, J. Galon, *Immunity* 39 (2013) 782–795.

- [19] M.S. Lawrence, P. Stojanov, P. Polak, G.V. Kryukov, K. Cibulskis, A. Sivachenko, S.L. Carter, C. Stewart, C.H. Mermel, S.A. Roberts, A. Kiezun, P.S. Hammerman, A. McKenna, Y. Drier, L. Zou, A.H. Ramos, T.J. Pugh, N. Stransky, E. Helman, J. Kim, C. Sougnez, L. Ambrogio, E. Nickerson, E. Shefler, M.L. Cortes, D. Auclair, G. Saksena, D. Voet, M. Noble, D. DiCara, P. Lin, L. Lichtenstein, D.I. Heiman, T. Fennell, M. Imielinski, B. Hernandez, E. Hodis, S. Baca, A.M. Dulak, J. Lohr, D. A. Landau, C.J. Wu, J. Melendez-Zajgla, A. Hidalgo-Miranda, A. Koren, S.A. McCarrroll, J. Mora, B. Crompton, R. Onofrio, M. Parkin, W. Winckler, K. Ardlie, S. B. Gabriel, C.W.M. Roberts, J.A. Biegel, K. Stegmaier, A.J. Bass, L.A. Garraway, M. Meyerson, T.R. Golub, D.A. Gordenin, S. Sunyaev, E.S. Lander, G. Getz, *Nature* 499 (2013) 214–218.
- [20] B. Seashore-Ludlow, M.G. Rees, J.H. Cheah, M. Cokol, E.V. Price, M.E. Coletti, V. Jones, N.E. Bodycombe, C.K. Soule, J. Gould, B. Alexander, A. Li, P. Montgomery, M.J. Wawer, N. Kuru, J.D. Kotz, C.S. Hon, B. Munoz, T. Liefeld, V. Dancik, J.A. Bittker, M. Palmer, J.E. Bradner, A.F. Shamji, P.A. Clemons, S. L. Schreiber, *Cancer Discov.* 5 (2015) 1210–1223.
- [21] P. Jiang, S. Gu, D. Pan, J. Fu, A. Sahu, X. Hu, Z. Li, N. Traugh, X. Bu, B. Li, J. Liu, G.J. Freeman, M.A. Brown, K.W. Wucherpfennig, X.S. Liu, *Nat. Med.* 24 (2018) 1550–1558.
- [22] T.W. Kim, D.H. Pyo, E. Ko, N.H. Yun, S.J. Song, S.M. Choi, H.K. Hong, S.H. Kim, Y.L. Choi, J. Lee, W.Y. Lee, Y.B. Cho, *Am. J. Cancer Res.* 12 (2022) 1393–1408.
- [23] B. Yang, Y.B. Ma, S.H. Chu, *Cancer Gene Ther.* 25 (2018) 309–316.
- [24] M.D. Nyquist, B. Prasad, E.A. Mostaghel, *Molecules* 22 (2017).
- [25] D.S. Chen, I. Mellman, *Nature* 541 (2017) 321–330.
- [26] S. Gao, L. Yan, R. Wang, J. Li, J. Yong, X. Zhou, Y. Wei, X. Wu, X. Wang, X. Fan, J. Yan, X. Zhi, Y. Gao, H. Guo, X. Jin, W. Wang, Y. Mao, F. Wang, L. Wen, W. Fu, H. Ge, J. Qiao, F. Tang, *Nat. Cell Biol.* 20 (2018) 721–734.
- [27] J. Guinney, R. Dienstmann, X. Wang, A. de Reynies, A. Schlicker, C. Soneson, L. Marisa, P. Roepman, G. Nyamundanda, P. Angelino, B.M. Bot, J.S. Morris, I. M. Simon, S. Gerster, E. Fessler, E.M.F. De Sousa, E. Missiaglia, H. Ramay, D. Barras, K. Homicsko, D. Maru, G.C. Manyam, B. Broom, V. Boige, B. Perez-Villamil, T. Laderas, R. Salazar, J.W. Gray, D. Hanahan, J. Taberner, R. Bernards, S.H. Friend, P. Laurent-Puig, J.P. Medema, A. Sadanandam, L. Wessels, M. Delorenzi, S. Kopetz, L. Vermeulen, S. Tejpar, *Nat. Med.* 21 (2015) 1350–1356.
- [28] L. Marisa, A. de Reynies, A. Duval, J. Selves, M.P. Gaub, L. Vescovo, M.C. Etienne-Grimaldi, R. Schiappa, D. Guenet, M. Ayadi, S. Kirzin, M. Chazal, J.F. Flejou, D. Benchimol, A. Berger, A. Lagarde, E. Pencreach, F. Piard, D. Elias, Y. Parc, S. Olschwang, G. Milano, P. Laurent-Puig, V. Boige, *PLoS Med.* 10 (2013), e1001453.
- [29] R. Zhou, D. Zeng, J. Zhang, H. Sun, J. Wu, N. Li, L. Liang, M. Shi, J. Bin, Y. Liao, N. Huang, W. Liao, *EBioMedicine* 42 (2019) 420–430.
- [30] R. Zhou, H. Sun, S. Zheng, J. Zhang, D. Zeng, J. Wu, Z. Huang, X. Rong, J. Bin, Y. Liao, M. Shi, W. Liao, *J. Cell Mol. Med.* 24 (2020) 3229–3241.
- [31] S. Mariathasan, S.J. Turley, D. Nickles, A. Castiglioni, K. Yuen, Y. Wang, E.E. Kadel III, H. Koepfen, J.L. Astarita, R. Cubas, S. Jhunjhunwala, R. Banchereau, Y. Yang, Y. Guan, C. Chalouni, J. Ziai, Y. Senbabaoglu, S. Santoro, D. Sheinson, J. Hung, J.M. Giltman, A.A. Pierce, K. Mesh, S. Lianoglou, J. Riegler, R.A. D. Carano, P. Eriksson, M. Hoggund, L. Somarrriba, D.L. Halligan, M.S. van der Heijden, Y. Loriot, J.E. Rosenberg, L. Fong, I. Mellman, D.S. Chen, M. Green, C. Derleth, G.D. Fine, P.S. Hegde, R. Bourgon, T. Powles, *Nature* 554 (2018) 544–548.
- [32] J. Xie, X.Y. Zhu, L.M. Liu, Z.Q. Meng, *Cancer Manag. Res.* 10 (2018) 153–166.
- [33] W. Dai, Y. Xu, S. Mo, Q. Li, J. Yu, R. Wang, Y. Ma, Y. Ni, W. Xiang, L. Han, L. Zhang, S. Cai, J. Qin, W.L. Chen, W. Jia, G. Cai, *Signal Transduct. Targeted Ther.* 5 (2020) 177.
- [34] M. Kim, S.H. Ly, Y. Xie, G.N. Duronio, D. Ford-Roshon, J.H. Hwang, R. Sulahian, J.P. Rennhack, J. So, O. Gjoerup, J.A. Talamas, M. Grandclaudon, H.W. Long, J. G. Doench, N.S. Sethi, M. Giannakis, W.C. Hahn, *Dev. Cell* 57 (2022) 212–227 e218.
- [35] C.C. Kuo, H.H. Ling, M.C. Chiang, C.H. Chung, W.Y. Lee, C.Y. Chu, Y.C. Wu, C.H. Chen, Y.W. Lai, I.L. Tsai, C.H. Cheng, C.W. Lin, *Theranostics* 9 (2019) 2526–2540.
- [36] A. Grothey, M. Fakhri, J. Taberner, *Ann. Oncol. : Offl. J. Eur. Soc. Med. Oncol.* 32 (2021) 959–967.
- [37] K. Okunushi, T. Furihata, H. Morio, Y. Muto, K. Higuchi, M. Kaneko, Y. Otsuka, Y. Ohno, Y. Watanabe, Y. Reien, K. Nakagawa, S. Sakamoto, H. Wakashin, N. Shimajo, N. Anzai, *J. Pharmacol. Sci.* 144 (2020) 16–22.
- [38] M. Belouche-Babari, T. Casals Galobart, T. Delgado-Goni, S. Wantuch, H.G. Parkes, D. Tandy, J.A. Harker, M.O. Leach, *Br. J. Cancer* 122 (2020) 895–903.
- [39] H. Ma, Z. Wu, J. Peng, Y. Li, H. Huang, Y. Liao, M. Zhou, L. Sun, N. Huang, M. Shi, J. Bin, Y. Liao, J. Rao, L. Wang, W. Liao, *Int. J. Cancer* 142 (2018) 2578–2588.
- [40] S. Panda, N. Banerjee, S. Chatterjee, *Drug Discov. Today* 25 (2020) 891–900.
- [41] X. Cheng, L. Wei, X. Huang, J. Zheng, M. Shao, T. Feng, J. Li, Y. Han, W. Tan, W. Tan, D. Lin, C. Wu, *Gastroenterology* 152 (2017) 1985–1997, e1912.
- [42] S. Xia, J. Wu, W. Zhou, M. Zhang, K. Zhao, J. Liu, D. Tian, J. Liao, *Cell Death Dis.* 12 (2021) 570.
- [43] L. Fang, D. Ford-Roshon, M. Russo, C. O'Brien, X. Xiong, C. Gurjao, M. Grandclaudon, S. Raghavan, S.M. Corsello, S.A. Carr, N.D. Udeshi, J. Berstler, E. Sicinska, K. Ng, M. Giannakis, *Nat. Commun.* 13 (2022) 3181.